THE QUIET CORONA: TEMPERATURE AND TEMPERATURE GRADIENT*

S. J. BAME, J. R. ASBRIDGE, W. C. FELDMAN
University of California, Los Alamos Scientific Laboratory, Los Alamos, N.M. 87544, U.S.A.

and

P. D. KEARNEY
Dept. of Physics, Colorado State University, Fort Collins, Colo. 80521, U.S.A.

(Received 21 November, 1973)

Abstract. A study of the lower corona thermal properties was made using the best examples of solar wind heavy ion spectra obtained with Vela 5 and 6 plasma analyzers at times of quiet solar wind (low speed, low temperature). The multiple Si and Fe ion species peaks in the spectra were fit with solutions of the ionization equilibrium equations to determine 'freezing in' temperatures for the various species over a range of heliocentric distances r. Assuming a power law electron temperature model, $T = T_\odot (R_\odot/r)^\alpha$, spherical symmetry, and mass conservation, the following results for the quiet corona were obtained: (1) The average freezing in temperatures ranged near 1.5×10^6 K at $r \simeq 2.4$ to 3.9 $R_\odot$. (2) Values for $T_\odot$ ranged between 1.7×10^6 K and 2.5×10^6 K with an average of $1.84 \pm 0.13 \times 10^6$ K. (3) The temperature gradient parameter α lay between 0.20 and 0.41 with an average value of $0.29 \pm \pm 0.06$. This is consistent with the predicted value $\alpha = 2/7$ derived from conduction dominated spherically symmetric models of the corona. (4) The 0 and N lines which freeze in at a distance of $r \simeq 1.5\ R_\odot$ indicate temperatures of $\sim 2.1 \times 10^6$ K. Temperatures higher at 1.5 $R_\odot$ than at 3 $R_\odot$, in agreement with extrapolations of the power law model, suggest that coronal heating in regions of open field geometry is not important beyond $r \simeq 1.5\ R_\odot$.

1. Introduction

One of the motivations for studying the solar wind at 1 AU is to obtain an understanding of the dominant physical processes in the solar corona which drive the supersonic solar wind. However, most properties of the plasma, as observed at 1 AU, have changed so much in transit from the Sun that it is very difficult to reconstruct the conditions in the corona responsible for its acceleration. Thus it is of great importance to identify and study those characteristics which remain unaltered in transit to the Earth from their values fixed low in the corona. Some properties of the interplanetary plasma which 'freeze in' at low coronal altitudes are the abundances and the ionization states of the heavy ions in the solar wind such as those of oxygen (Bame *et al.*, 1968) and silicon and iron (Bame *et al.*, 1970). Quantitative determinations of the thermal state of the lower corona can be made from the measured ionization states (Hundhausen *et al.*, 1968a and b). This paper gives a comprehensive treatment of the quiet corona temperature and temperature gradient determined from an analysis of the best heavy ion spectra observed with electrostatic analyzers on the Vela 5A, 5B, 6A and 6B spacecraft.

Solar Physics **35** (1974) 137–152. *All Rights Reserved*

A review of studies of the solar wind heavy ion content has been given by Bame (1972). It is evident that a wealth of information concerning the state of the lower corona is carried by the plasma heavy ion component. In particular, a Vela 5A heavy ion energy per charge spectrum measured in 1969, July 6, was analyzed to determine the temperature and temperature gradient in the corona 1 and 1/2 solar radii above the photosphere (see also Bame *et al.*, 1970). This determination was inferred from the measured relative abundance of the iron ionization species, Fe^i, with $7+ \leqslant i \leqslant 12+$, since the ratios $n(Fe^{i+1})/n(Fe^i)$ become set or 'freeze in' at different coronal altitudes for different values of i. The results for this one spectrum gave rough values of T_e at 2.5 $R_\odot$ and $\alpha = -\mathrm{d}\ln T_e/\mathrm{d}\ln r$ of about 1.58×10^6 K and 0.24. Here T_e is the coronal electron temperature, $R_\odot$ is the solar radius, r is the heliocentric radius, and α is the power law index, defined further later.

To get a more accurate picture of the average coronal conditions and to study their variability it is of interest to repeat this determination for as many examples as possible and to make a careful analysis of the errors. A limited number of examples suitable for detailed analysis have been found among the E/q spectra measured by the Vela 5 and 6 heavy ion electrostatic analyzers between June 1969 and March 1972. The selected E/q spectra were obtained during times when the ion temperatures were low, a condition necessary to be able to resolve individual ion species with an electrostatic analysis alone.

Two mutually distinct categories of solar wind plasma have the required low ion temperatures. The first is sometimes observed $\sim\frac{1}{2}$ day after solar flare generated shock waves arrive near earth. During the passage of the flare piston gas, the ion and electron temperatures fall to very low values even though the speed need not be low (Gosling *et al.*, 1973; Montgomery *et al.*, 1972; Montgomery *et al.*, in preparation). This plasma has a heavy ion signature characteristic of solar flares or other energetic coronal events (Bame *et al.*, 1973; Bame *et al.*, in preparation).

The second category is obtained in what is commonly termed 'quiet' solar wind flow when the speed is low and the proton temperature has its expected low values (Strong *et al.*, 1966; Hundhausen *et al.*, 1970; Burlaga and Ogilvie, 1970). This plasma has a heavy ion signature characteristic of quiet coronal conditions. Studies based on spectra measured at these times furnish information concerning heavy ion abundances and their relative variations (Kearney *et al.*, in preparation), the solar wind He^+ content at 1 AU (Kearney *et al.*, 1973; Feldman *et al.*, in preparation), and the electron thermal state of the lower corona for quiet conditions, considered in this paper.

2. Instrumentation and Data Selection

The results to be reported here were measured with the Vela 5 and 6 heavy ion and standard solar wind electrostatic analyzers between June 1969 and March 1972. A description of the instrumentation and data accumulation cycle is presented elsewhere (Bame *et al.*, 1970; Bame, 1972). Due to the nature of the instruments, orbits, spacecraft orientation, tracking schedule and other severe constraints, very few E/q spectra

are suitable for analysis. The numerous factors bearing on the usefulness of a heavy ion measurement are detailed by Bame (1972). (See also Feldman *et al.*, in preparation) In particular, as previously mentioned, the solar wind temperature must be low to be able to resolve the heavy ion species.

Between June 1969 and March 1972 nineteen heavy ion E/q spectra in the quiet flow condition class were deemed suitable for analysis of relative species abundances. However, to make a meaningful determination of the temperature and temperature gradient in the lower corona, the flux of heavy ions must be large enough that adequate statistics are obtained for each of the measured Fe^{7+} to Fe^{13+} and Si^{7+} to Si^{9+} ion species peaks. For this reason only five of these spectra are used here; one of them, the July 6, 1969 spectrum can be found in Bame *et al.* (1970) (see also Bame, 1972) and the remaining four, measured on the specified dates, are shown in Figure 1.

3. Data Analysis

The peaks are identified in Figure 1 according to their respective M/q locations which are directly derived from the measured E/q spectra assuming all species travel with the same bulk speed. Such an assumption has given consistent results in past Vela studies. However, in light of the recently discovered double streams of ions occasionally observed in the solar wind (Feldman *et al.*, 1973), a review of the evidence for a single flow speed and proper identification at these times should be given.

The assumption is justified on several grounds. (1) The proton peaks measured with the conventional solar wind analyzer on each spacecraft do not have secondary peaks below the He^{2+} peak. There is thus no evidence for double ion streaming during the time periods of interest here. (2) In addition to purely electrostatic analysis the Vela instruments perform a rough pulse height analysis on secondary electron pulses produced by the ions which provides information concerning ion mass. For example, Vela 3 measurements were the first to demonstrate that ions in the presumed He^{2+} peaks observed in solar wind spectra were indeed more massive than protons (Bame *et al.*, 1968). Similarly it can be demonstrated that the ions producing the presumed heavy ion peaks in the Vela 3, 5, and 6 spectra are more massive than He^{2+}. (3) Finally, the assumption of a single flow speed produces such a self consistent result in locating the various ion peaks that any other interpretation is completely unrealistic (see also Feldman *et al.*, to be published).

As can be noted in Figure 1, identification on the basis of M/q is not unambiguous. For example, measureable contributions to the peak at $M/q=4$ may be expected from Si^{7+}, S^{8+}, Ca^{10+} and He^{+} among others. In addition Si^{8+} and S^{9+} both contribute to the $M/q \cong 3.5$ peak; Si^{9+}, S^{10+} and perhaps those of Mg^{8+} contribute to the $M/q=3.1$ peak, etc. More details and tables of abundances and M/q values can be found in Holzer and Axford (1970); Lange and Scherb (1970); and Bame (1972). However the iron ionization peaks are expected to be relatively pure with no more than a $\sim 5\%$ contribution due to Ni ions. Thus to obtain the most accuracy for the temperature and temperature gradient in the lower corona, values are determined

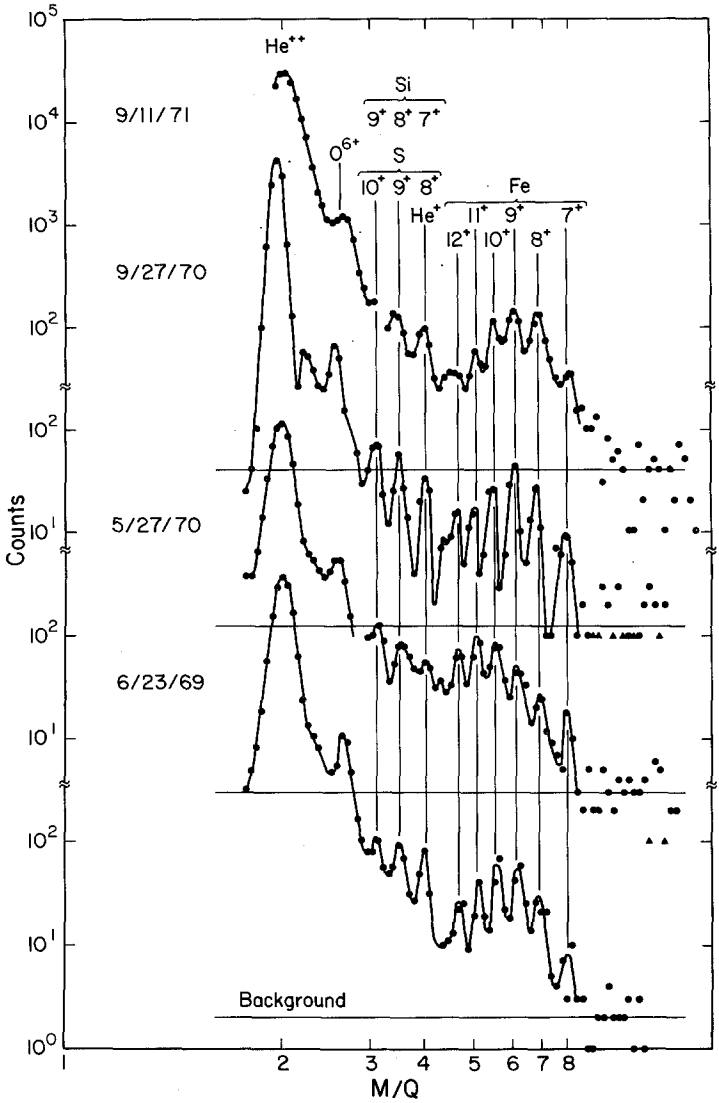

Fig. 1. Four of the five solar wind heavy ion spectra selected for study. The M/Q scale is established assuming all ion species have a common bulk speed. Vertical lines give positions of the more abundant species.

using the Fe peaks and Si^{8+} and Si^{9+} peaks alone, with appropriate corrections made for the presence of S^{9+} and S^{10+} in the silicon peak positions.

The simplest model for the thermal state of the lower corona, $1.5\ R_\odot \lesssim r \lesssim 3.5\ R_\odot$, is to assume T_e = constant. Such an isothermal model was used to give an approximate characterization of the heavy ion spectrum measured using the Vela 5 instrument on July 6, 1969 (Bame *et al.*, 1970; Bame, 1972). The theoretical temperature dependent ionization state calculations for Fe and Si published by Jordan (1969) and Allen and

Dupree (1969) were used to obtain a best fit of the data, as judged by eye, of $T_e \cong$ $\cong 1.5 \times 10^6$ K. It was noted that use of Jordan's density dependent coefficients gave ionization state envelopes similar to those determined by Allen and Dupree but for temperatures about 0.25×10^6 K lower. However, for quiet conditions the ion state freezes in at $r \approx 3\ R_\odot$ where the electron density and the expansion rate are low enough that the density independent coefficients are more suitable. Both ionization state calculations then yield equivalent coronal electron temperatures. However, the fit of the theoretical envelopes to the data showed that the experimental envelope of the iron ionization state was broader than the single temperature theory predicts. This effect was attributed to the failure of the isothermal model to adequately describe the expanding corona.

Departures from predictions of an isothermal model may result from coronal electron temperature variations associated with either temporal or spatial variations in the expanding corona. The rates for establishing equilibrium among the ion species of a given element, such as iron, differ for the different ionization stages. If all of these scale times are shorter than the scale time of the temperature variations, whether the variations are temporal or spatial, the ionization state will adjust to the instantaneous electron temperature. However, if the time scales for establishment of some of the ionization stages become comparable to or longer than the time scale for temperature variations, departures from ionization equilibrium will occur.

A temperature variation at $\approx 3\ R_\odot$ may be due to a spatial temperature gradient in the corona and interplanetary space. Near the Earth $T_e \approx 1.5 \times 10^5$ K, whereas in the corona it is $\approx 1.5 \times 10^6$ K; the gradient can be easily modelled. The plasma ionization state observed at 1 AU is determined as the coronal gas expands over a range of altitudes where the scale times for the establishment of the stages of ionization rise above the expansion scale time $[V\ \mathrm{d} \ln n_e/\mathrm{d}r]^{-1}$. For a typical iron ionization state populated at $T_e \approx 1.5 \times 10^6$ K this occurs over a range of heliocentric distances near $r \approx 3\ R_\odot$. Since the various species decouple or freeze in/at different altitudes, deviations from an isothermal prediction are expected.

Temporal temperature fluctuations might arise from local energy deposition due to the dissipation of shock waves generated by disturbances in the hydrogen convection zone (House and Billings, 1964). It is not known whether shock waves or other temporal effects contributing to heating of the corona exist in the solar atmosphere at $r \approx 3\ R_\odot$. Although some evidence has been published to infer coronal heating out to distances of $\approx 20\ R_\odot$ (Sturrock and Hartle, 1966; Hartle and Sturrock, 1968; Parker, 1965; Barnes et al., 1971; Hundhausen, 1972), this point is not firmly established. Thus, in the following analysis only the temperature variation due to a spatial gradient will be considered.

The five heavy ion spectra measured between June 1969 and March 1972 with best statistics in the multiple Si and Fe ion peaks were fit with solutions of the dynamic ionization equilibrium equations to determine the coronal temperature, temperature gradient, and information on the ion composition. The coronal temperature gradient was modelled using the power law radial dependence,

$$T = T_{\odot}\left(\frac{R_{\odot}}{r}\right)^{\alpha},$$

where $T_{\odot}$ is the coronal electron temperature at $r=1\ R_{\odot}$. This model, of course, must break down at very low altitudes, but should be adequate in the 2.5 $R_{\odot}$ to 4 $R_{\odot}$ range where the heavier ion states are set. Using the assumptions of spherical symmetry and mass conservation, the dynamic equations of ionization equilibrium can be written in the form

$$\frac{\mathrm{d}\,(n_i/n_e)}{\mathrm{d}\ln\chi} = \frac{n_e^2\chi^3 R_{\odot}}{F}\left[\frac{n_{i-1}}{n_e}C_{i-1} - \frac{n_i}{n_e}(C_i + R_i) + \frac{n_{i+1}}{n_e}R_{i+1}\right], \tag{1}$$

where n_i is the relative abundance of the ith ionization state of a particular element (e.g., Fe), n_e is the local electron number density, $\chi = r/R_{\odot}$, $F = n_e V \chi^2$ is constant for spherical symmetry, V is the solar wind bulk speed, $C_i(T)$ is the collisional ionization coefficient from ionization state i and $R_i(T)$ is the radiative recombination coefficient to ionization state $i-1$ including dielectronic recombination*. The representative coronal electron densities tabulated by Newkirk (1967) were used in (1) to obtain solutions for the n_i of Fe and Si evaluated at $r=1$ AU for $1.2\times10^6\ K \leqslant T_{\odot} \leqslant 3.27\times10^6$ K and $0 \leqslant \alpha \leqslant 0.6$. The solutions of Equation (1) for n_i/n_e at 1 AU are very sensitive to these assumed densities. Although the densities of coronal regions from which the solar wind plasma originates are not presently known with precision and may be different from the values tabulated by Newkirk, his model is the best presently available for the 'quiet' corona (see Section 4 for a discussion of this point).

In a static situation, the equilibrium between successive stages of ionization of a given species is given by

$$n_i/n_{i+1} = R_{i+1}/C_i$$

The number of ionizing collisions of stage i per i particle per second $= n_e C_i = \tau_c^{-1}$ and the number of recombinations from stage $i+1$ to stage i per $i+1$ particle per second $= n_e R_{i+1} = \tau_n^{-1}$. When τ_c and τ_n become longer than the expansion scale time, $\tau_e = (V d\ln n/\mathrm{d}r)^{-1}$, the plasma can no longer be considered static. At this point the ratio between ionization stages i and $i+1$ can no longer adjust to changes in the local plasma temperature and thus is said to be frozen. Setting $V = F/n_e\chi^2$ with F = constant calculated at 1 AU, $T_e(r) = T_{\odot}(R_{\odot}/r)^{\alpha}$ with $T_{\odot} = 2\times10^6$ and $\alpha = 0.3$ and using the n_e tabulated by Newkirk (1967), these time scales are compared for Fe^{10+} and Fe^{11+} in Figure 2. It is readily seen that the ratio $n(Fe^{10+})/n(Fe^{11+})$ freezes in at $r \approx 3\ R_{\odot}$. Repeating this analysis for the other Fe ionization stages as well as for those of Si and O shows that the radial freezing in base line for Fe extends from 3.9 $R_{\odot}$ (Fe^{7+}) to 2.6 $R_{\odot}$ (Fe^{13+}), whereas the Si ionization stages freeze in between 2.8 $R_{\odot}$ (Si^{7+}) and 2.4 $R_{\odot}$ (Si^{9+}) and the $O^{7+}-O^{6+}$ ratio freezes in at about 1.5 $R_{\odot}$. (See also Hundhausen *et al.*, 1968a, b).

* We wish to thank Dr A. Dupree for kindly supplying us with the C and R coefficients for Fe, Si and O as a function of T.

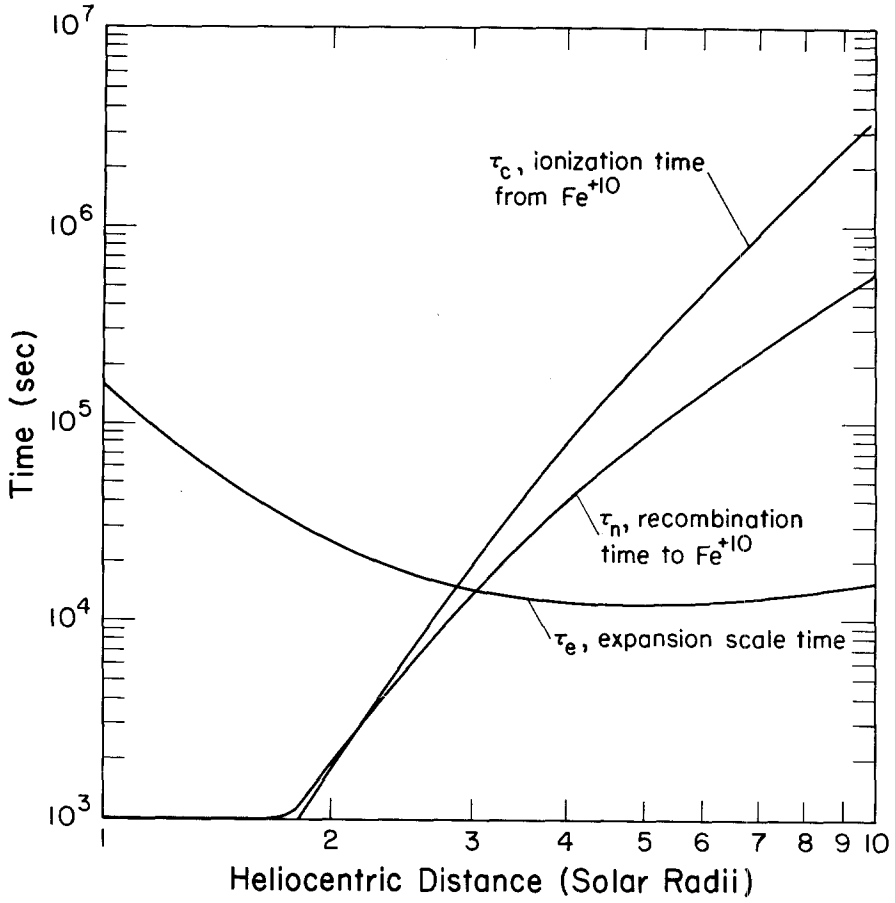

Fig. 2. Scale times for the ionization of Fe^{+10}, the recombination of Fe^{+11}, and the expansion through a density scale height, as a function of heliocentric distance.

From the above it is apparent that the best values of T_e and dT_e/dr can in principle be obtained using the fullest set of ion species extending from O^{7+} to Fe^{7+}. This would provide the longest radial baseline of freezing in positions and the best statistics. In practice the ionization stages O^{7+}, O^{6+}, and Si^{7+} were eliminated from the analysis because of contamination of the O^{7+} species with N^{6+}, C^{5+} and Mg^{10+} and of the Si^{7+} species with S^{8+}, Ca^{10+}, Ar^{9+} and possibly other species. Even though the Si^{8+} and Si^{9+} species are contaminated with S^{9+} and S^{10+}, it is possible to adequately account for the contamination, so these peaks along with the Fe peaks of the selected spectra were used to determine $T_\odot$ and α.

To effect the comparison with theory, sums of counts for the three E/q samples bracketting each of the Si and Fe peaks accepted for analysis were tabulated and used to represent the relative ionization state abundances. An assumed constant background, estimated using E/q levels above the Fe^{7+} peak (and indicated in Figure 1) was substracted from each of the above sums. The procedure is justified if the measur-

ed line shapes (with respect to $\log(E/q)$) for all the Si and Fe peaks are the same. The line shapes of the peaks in Figure 1 seem to be the same within experimental accuracy where they can be checked. Error bars were assigned to each sum from the counting statistics alone.

Values for $T_\odot$ and α were obtained by fitting the predicted relative abundances of the Fe and Si ion species to the above sums using the method of least squares in two iterations. The first used the Fe peaks alone. The coronal temperature T_i resulting from the best isothermal model ($\alpha=0$) fit was then used to establish the S ion abundances so that the S contamination could be removed from the Si ion peaks using $0.2 \leqslant n(\mathrm{S})/n(\mathrm{Si}) \leqslant 0.8$. The relative abundances of the S ions for T_i were obtained from Jordan (1969). A second fit to the combined Fe and Si peaks then yielded the best α, $T_\odot$ and Si-Fe abundance ratios.

A map of the two-dimensional (in α, $T_\odot$ space) normalized chi-square surface generated by comparing the predicted n_i with those tabulated from the heavy ion spectrum measured on 1969, July 6 is reproduced in Figure 3. Here $n(\mathrm{S})/n(\mathrm{Si})=0.4$ is

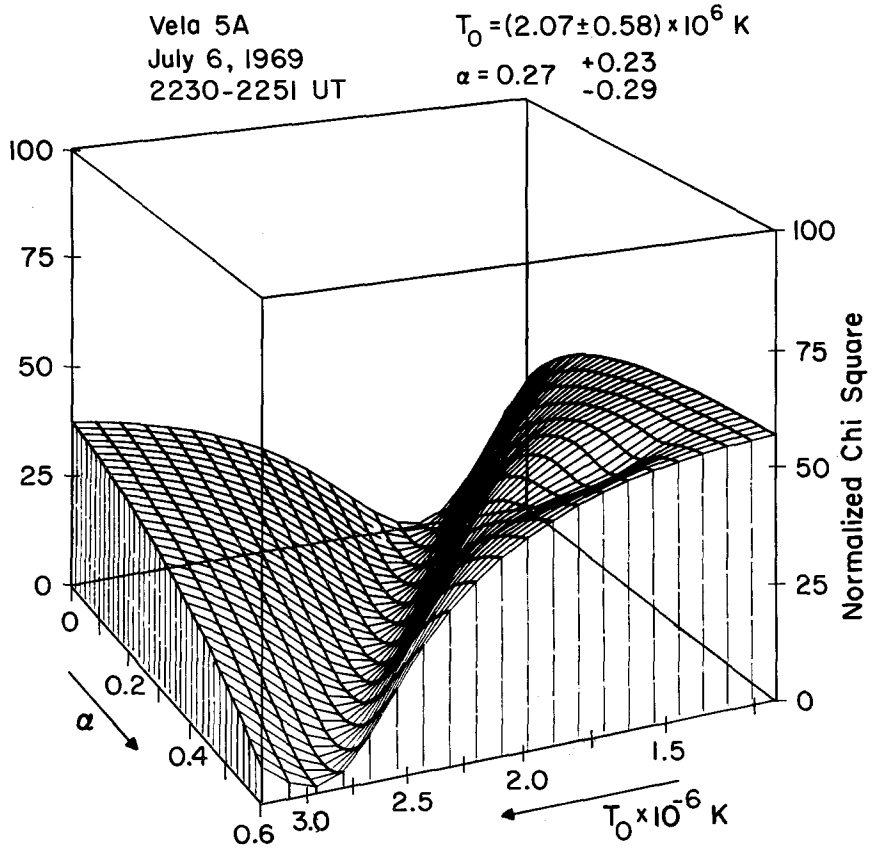

Fig. 3. Map of the two-dimensional normalized chi-square surface for the 1969, July 6, heavy ion spectrum.

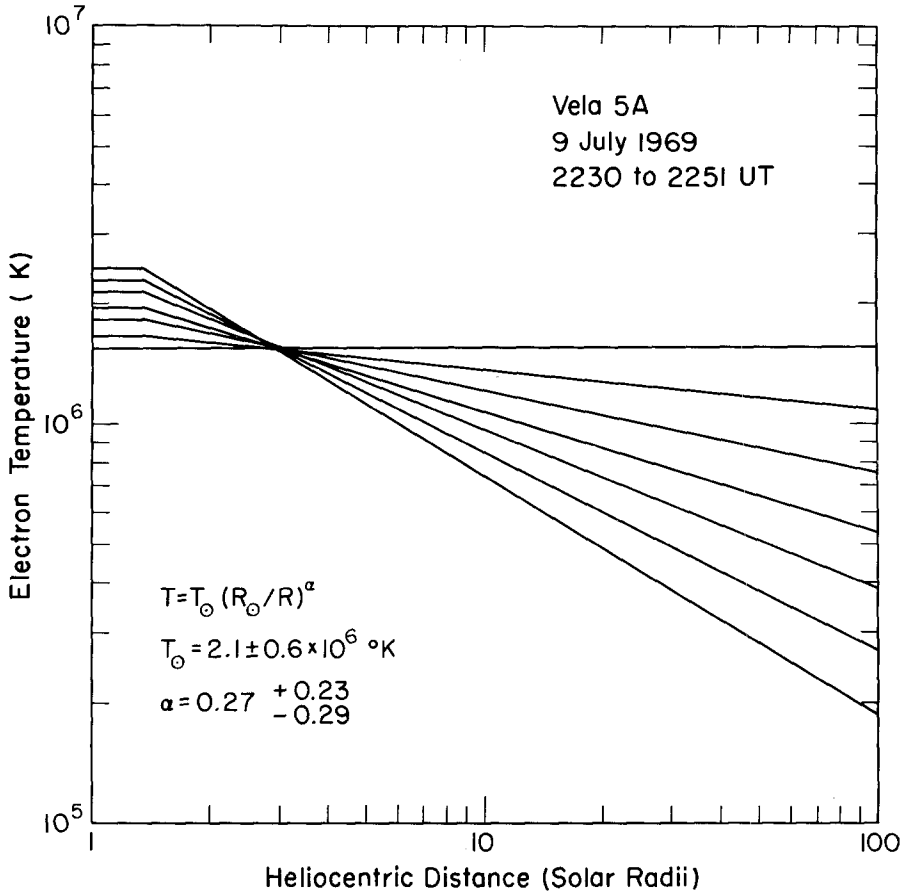

Fig. 4. Radial dependence of T for a few of the points along the chi-square valley shown in Figure 3.

assumed. It is readily seen that instead of having a well defined single minimum, χ^2 minimizes along a valley where α is proportional to $T_\odot$. The radial dependence of T, $T=T_\odot (R_\odot/r)^\alpha$, for a few of the points along this valley are shown in Figure 4. It is noticed at once that all the lines cross at $r=3\ R_\odot$. This is due to the fact that the Fe ionization states are dominated by Fe^{10+} which freezes in at $r \simeq 3\ R_\odot$. (See e.g., Figure 2) The fact that the other Fe ions as well as the Si ions freeze in at different radii enables a choice among the points along this valley. A plot of the normalized chi-square along the valley, as well as the dependence of α on $T_\odot$ for these points, are presented in Figure 5. A well defined, although broad minimum in χ^2 is apparent. The position of the minimum yields $\chi^2_{\min}=2.0$ with 4 degrees of freedom and $T_\odot = (2.1^{+0.8}_{-0.6}) \times 10^6$ K, $\alpha = 0.27 \pm 0.27$. The error bars for $T_\odot$ and α are generated by noting the values of the parameters where the line $\chi^2 = \chi^2_{\min} + 1$ intersects the curve $\chi^2(T_\odot)$ plotted in Figure 5 (Bevington, 1969). This follows since the valley has very steep walls.

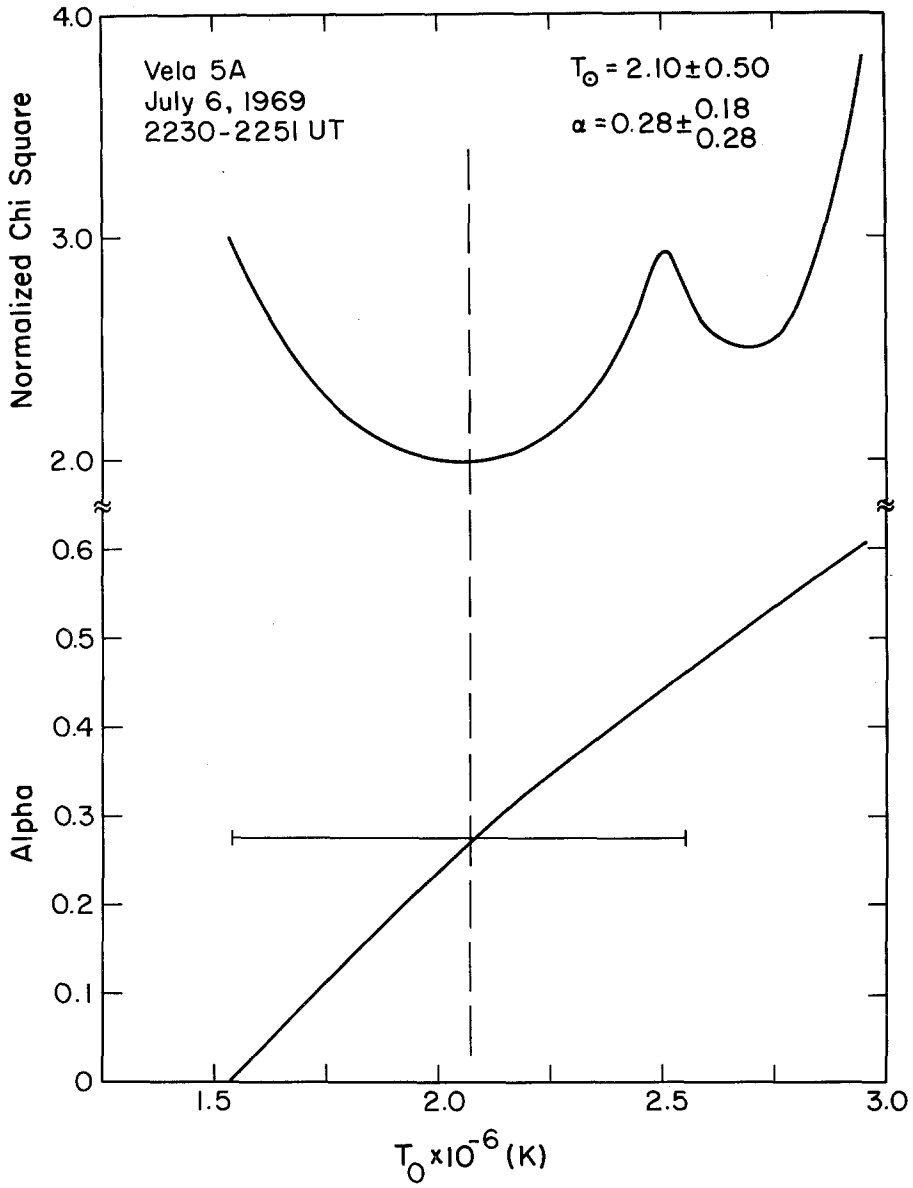

Fig. 5. Normalized chi-square and the dependence of α on $T_\odot$ along the valley shown in Figure 3.

Similar results are obtained by repeating the above procedure for $0.2 \leqslant n(S)/n(Si) \leqslant 0.8$ in steps of 0.2 and for the other four heavy ion E/q spectra. The results are summarized in Table I. Included in Table I in addition to $T_\odot$, α, and $T(3\ R_\odot)$ are $n(H)$, V and $n(He^{2+})/nH^+)$ determined from spectra measured simultaneously using the standard solar wind plasma analyzer also aboard the Vela spacecraft. Also included are $n(Fe)/n(H)$ determined from the total counts in the M/q region corresponding

TABLE I

Quiet coronal thermal and abundance characteristics from 5 accepted heavy ion spectrums

$\frac{n(S)}{n(Si}$	Date	$n(H^+)$ cm^{-3}	V km s^{-1}	$\frac{n(He^{2+})}{n(H^+)}$ $\times 10^{-2}$	$T_\odot$ $\times 10^6$ K	α	$T(3R_\odot)$ $\times 10^6$ K	$\frac{n(Fe)}{n(H)}$ $\times 10^{-5}$	$\frac{n(Si)}{n(Fe)}$	$\frac{n(Si)}{n(H)}$ $\times 10^{-5}$
0.2					1.8 $^{+0.4}_{-0.3}$	0.2 $\pm$0.18	1.47		1.29	9.5
0.4					1.8 $\pm$0.3	0.2 $^{+0.2}_{-0.18}$	1.47		1.15	8.4
	69/6/23	6	362	4.6				7.3		
0.6					1.89$\pm$0.35	0.23$^{+0.17}_{-0.20}$	1.47		1.09	7.9
0.8					1.98$^{+0.25}_{-0.45}$	0.28$^{+0.12}_{-0.23}$	1.47		0.99	7.2
0.2					1.93$^{+0.6}_{-0.4}$	0.21$^{+0.24}_{-0.21}$	1.54		1.60	6.5
0.4					2.1 $^{+0.8}_{-0.5}$	0.27$\pm$0.27	1.56		1.57	6.4
	69/7/06	25	293	3.0				4.1		
0.6					2.2 $\pm$0.6	0.32$^{+0.2}_{-0.29}$	1.56		1.38	5.7
0.8					2.2 $\pm$0.6	0.32$^{+0.25}_{-0.29}$	1.58		1.24	5.1
0.2					2.3 $\pm$0.5	0.33$^{+0.19}_{-0.23}$	1.62		1.14	10.4
0.4					2.4 $\pm$0.5	0.36$^{+0.24}_{-0.23}$	1.66		1.11	10.1
	70/5/27	8.6	333	1.8				9.1		
0.6					2.5 $^{+0.5}_{-0.6}$	0.41$^{+0.16}_{-0.28}$	1.64		0.98	8.9
0.8					2.5 $\pm$0.6	0.41$^{+0.19}_{-0.26}$	1.64		0.96	8.7
0.2					2.1 $^{+0.3}_{-0.2}$	0.38$\pm$0.11	1.38		1.83	8.2
0.4					2.1 $\pm$0.3	0.38$\pm$0.11	1.40		1.66	7.5
	70/9/27	5.1	343	5.3				4.5		
0.6					2.1 $\pm$0.3	0.38$^{+0.09}_{-0.13}$	1.43		1.52	6.8
0.8					2.1 $\pm$0.3	0.38$\pm$0.11	1.40		1.40	6.3
0.2					1.7 $^{+0.1}_{-0.25}$	0.25$^{+0.05}_{-0.13}$	1.28		0.73	8.8
0.4					1.7 $^{+0.1}_{-0.2}$	0.23$^{+0.07}_{-0.13}$	1.29		0.65	7.8
	71/9/11	10	315	4.3				12.0		
0.6					1.7 $^{+0.1}_{-0.2}$	0.23$^{+0.07}_{-0.13}$	1.30		0.58	7.0
0.8					1.7 $^{+0.1}_{-0.2}$	0.25$^{+0.07}_{-0.13}$	1.29		0.53	6.3
Average		10.9	329	4.2	1.84$\pm$0.13	0.29$\pm$0.06	1.48	7.4	1.23	8.0

to the lines of iron between Fe^{7+} and Fe^{13+} along with the known heavy ion analyzer characteristic. The ratio $n(Si)/n(Fe)$ and hence $n(Si)/n(H)$ is also determined from the above fitting procedure. The Fe and Si abundances resulting from the least-squares fitting procedure are listed in Table I only for completeness; a discussion of their magnitude and variations is presented in Kearney *et al.* (in preparation). The results listed in Table I pertaining to the quiet time coronal thermal structure will now be discussed.

4. Discussion

Both the solar wind bulk speed and temperature are necessarily low for all five spectra because of the selection criterion discussed earlier. The flow conditions at 1 AU are then expected to be characteristic of the 'quiet time' solar wind. Indeed inspection of three-hour averages of solar wind flow parameters as measured by the standard Vela plasma analyzers substantiates this conclusion. There may be some uncertainty in this characterization for 1969, July 6 as the heavy ion spectrum was accumulated just as the density began to rise in front of a high speed stream. However, the density wave at the leading edge of such streams really propagates in the ambient medium which, nearer the sun at $r \cong 3\ R_\odot$, would be characterized as a quiet time flow. It is then expected that the five heavy ion spectra are all examples of normal or quiet time coronal thermal boundary conditions. Thus, although the variations of parameters listed in Table I are considered real, averages of $T_\odot$ and α determined from each of the measurements have meaning as the best characterization of the thermal state of the quiet time corona near $r \cong 3\ R_\odot$.

In order to extend the radial baseline for a more accurate determination of dT/dr, the Si^{9+} and Si^{8+} abundances were included in the analysis. This required the subtraction of the S^{9+} and S^{10+} content from the appropriate M/q spectral peaks as described earlier. Although most determinations of the coronal sulfur to silicon abundance ratio yield values between 0.4 and 0.6 (see e.g., Noyes and Withbroe, 1972; Mewe, 1972; Dupree, 1972; Pottasch, 1967), it is useful to note the effect variations of $n(S)/n(Si)$ has on $T_\odot$ and α. Thus values for $T_\odot$ and α are listed in Table I for $0.2 \leqslant n(S)/n(Si) \leqslant 0.8$. It is readily noted that variations due to this effect are much smaller than the statistical error bars. Without loss of accuracy then, $n(S)/n(Si)$ is chosen equal to 0.4. Using this assumption, the best values for $T_\odot$ and α along with appropriate errors are listed on the bottom of Table I. Best values for a set of measured parameters P_k whose accuracy is specified by σ_k is given by (Bevington, 1969)

$$\langle P_k \rangle = \sum_k P_k/\sigma_k^2 / \sum_k 1/\sigma_k^2 .$$

Thus $\langle T_\odot \rangle = (1.84 \pm 0.13) \times 10^6$ K and $\langle \alpha \rangle = 0.29 \pm 0.06$. It is necessary to note that although the power law temperature model yields a value for the coronal electron temperature evaluated at $r = R_\odot$, the temperature is effectively sampled at $r = 3\ R_\odot$. Therefore $T(3\ R_\odot)$ is also listed in Table I: $\langle T(3\ R_\odot) \rangle = 1.48 \times 10^6$ K.

The coronal temperature gradient near to the Sun but beyond the temperature maximum has been determined from the radial dependence of the widths of forbidden

emission lines (see e.g., Billings, 1966) and of the ratio of Fex (λ6374) to Fexiv (λ5303) line intensities (Athay, 1973). Whereas Billings determined a thermal gradient of $\simeq 2$ K per km which corresponds to $\alpha \simeq 0.7$, Athay found $\alpha \lesssim 0.07$. These determinations are to be compared with the value for α obtained here from solar wind heavy ion spectra: $\alpha = 0.29 \pm 0.06$. The discrepancy may be due to the fact that while contributions to the line intensity recorded on an eclipse photograph come from a large volume of perhaps inhomogeneous coronal plasma, a solar wind heavy ion measurement samples a very small volume of coronal plasma. Furthermore it seems likely that a large fraction of the light samples in an eclipse photograph comes from plasma which lies within quasistatic closed magnetic structures which do not expand into interplanetary space. The thermal gradient in a static volume of the corona may well be quite different from that in a volume which is connected to 1 AU through the interplanetary magnetic field.

The average value determined here for the thermal gradient parameter, α, is in good agreement with the value predicted for a heat conduction dominated spherically symmetric corona: $\alpha = 2/7$ (Chapman, 1957). Of course there are other terms in the electron energy equation besides the conduction term, $\kappa \mathrm{d}T/\mathrm{d}r$, but they are expected to be small at $r = 3\ R_\odot$. This result then implies that the heating of the quiet coronal electron component takes place inside of $r = 3\ R_\odot$ and makes the analysis self consistent.

Since the maximum radius of major coronal heating is a basic parameter needed for an understanding of coronal physics, it is important to try to localize the radius of maximum electron temperature further. In principle this problem can be approached by determining the freezing in temperatures for ion pairs whose ratios are established at as low a value of r as possible. Such a pair is O^{7+} and O^{6+} but often O^{7+} is obscured by He^{2+} (see Figure 1). Even when it is well resolved the O^{7+} peak is contaminated with ions of N^{6+}, C^{5+}, and Mg^{10+}, so that the abundance ratio of this pair cannot be determined with high accuracy. Fortunately, a similar analysis can be made by including the species near O^{7+} and determining the abundance ratio $n(O^{7+} + N^{6+} + C^{5+} + Mg^{10+})/n(O^{6+})$. For a few cases such as the spectrum measured on 1970, September 7 the O^{7+} group is resolved. Here the peak lying between the He^{2+} and O^{6+} peaks is situated exactly where O^{7+}, with some contamination of the expected species, should be found. The location and shape (broadened on one side) argue for dominant contributions from O^{7+} and N^{6+} and lesser contributions of C^{5+} and Mg^{10+}. A search through the remaining 14 heavy ion spectra selected from those measured between June 1969 and March 1972 yielded two others, measured on 1969, June 22 and 1970, November 22, which had resolved $(O^{7+} + N^{6+} + C^{5+} + Mg^{10+})$ peaks. Although these spectra had insufficient statistics in their Si and Fe peaks and so were not used for the earlier analysis of T_e and $\mathrm{d}T_e/\mathrm{d}r$, they are useful here. Values calculated for $n(O^{7+} + N^{6+} + C^{5+} + Mg^{10+})/n(O^{6+})$ using abundance ratios tabulated by Noyes and Withbroe (1972) and Mewe (1972) along with the relative ionization state populations tabulated by Jordan (1969) are listed in Table II for $T_e = 1.58 \times 10^6$ K, 2.0×10^6 K, and 2.5×10^6 K. Values for this ratio measured from the above three

TABLE II

Predicted and measured abundance ratio $n(O^{7+}+N^{6+}+C^{5+}+Mg^{10+})/n(O^{6+})$

$T\times10^{-6}$ K	Noyes and Withbroe	Mewe	69/6/22	70/9/27	70/11/22
1.58	0.65	0.75			
2.0	1.06	1.13	1.5	1.25	1.34
2.5	2.0	2.10			
		Best T	2.2×10^6 K	2.1×10^6 K	2.1×10^6 K

heavy ion spectra are also tabulated. Indeed, all three measured ratios seem most consistent with a freezing in temperature of $\simeq 2.1\times10^6$ K. This value is higher than the average freezing in temperature of the Fe and Si lines listed in Table I. In fact, for the one spectrum common to Tables I and II, 1970, September 27, the temperature appropriate to the freezing in position of O^{7+} and N^{6+}, $T(1.5R_\odot)=2.1\times10^6$ K, agrees very well with the model temperature $T(R_\odot)=2.1\pm0.3\times10^6$ K. This agreement appears to be strong evidence for the maximum quiet time coronal electron temperature to be located well inside of 3 $R_\odot$ and probably inside of 1.5 $R_\odot$.

Possible coronal heating mechanisms have been explored in detail by Kuperus (1969). If energy is transferred from the photosphere to the corona in the form of mechanical waves which steepen into shocks as they propagate upwards, the proton plasma component should absorb most of the energy. This energy will be equipartitioned between the proton and electron components by coulomb energy transfer collisions as long as the coulomb energy transfer time, τ_c is much smaller than the coronal expansion time, τ_e. These two quantities are readily evaluated at $r=1.5\ R_\odot$ using the electron densities tabulated by Newkirk (1967) and assuming $T\simeq2.1\times10^6$ K: $\tau_c\simeq650\text{ s}\ll\tau_e\simeq4\times10^4$ s. The resulting tight thermal coupling between plasma proton and electron components at 1.5 $R_\odot$ then requires nearly equal proton and electron temperatures, $T_p\simeq T_e$. Since the maximum T_e for quiet time coronal conditions has been determined to be located inside $r=1.5\ R_\odot$, the same must be true for T_p. This then implies that the maximum radius of major coronal heating, r_m, is $\lesssim1.5\ R_\odot$. This value for r_m is consistent with the outer limit of coronal heating expected from theories of shock heating assuming shock wave periods of $\simeq300$ s (Kopp, 1968).

A few cautionary notes should be considered with regard to the results reported in this paper. First, solar wind flow may arise from only limited regions of the corona due to the extremely complicated closed magnetic structures observed close to the Sun (Davis, 1965; Schatten *et al.*, 1969; Altschuler and Newkirk, 1969; Schatten, 1971). Thus the assumption of spherical symmetry used to derive Equation (1) may not be valid for small r. However, beyond 2.5 $R_\odot$ it may be a reasonable assumption since the plasma energy density begins to dominate the transverse magnetic field energy density and forces the flow to become radial. Indeed, comparison of calculated coronal fields using the measured photospheric field as a boundary condition yields best fits to interplanetary measurements (Schatten *et al.*, 1969; Schatten, 1972) and the morphology of coronal density structures (Altschuler and Newkirk, 1969; Newkirk, 1972) if the field is

required to be nearly radial on a sphere of radius R_W with $1.6 \lesssim R_W \lesssim 2.5\ R_\odot$. Since the freezing in distances, R_F, of the Si and Fe ionization states lie in the interval $2.4 \leqslant \leqslant R_F \leqslant 3.9\ R_\odot$, the assumption of spherical symmetry used to derive Equation (1) may be valid for the analysis presented here.

Secondly, it is difficult to assess the applicability of Newkirk's density model (Newkirk, 1967) to the portions of the corona connected to 1 AU through the solar wind flow. Presently, high speed streams are thought to originate in coronal holes which may be as much as a factor of 5 less dense at the coronal base than is indicated by Newkirk's model (Withbroe *et al.*, 1971; Altschuler *et al.*, 1972; Krieger *et al.*, 1973). However, the solar wind samples presented here are characteristic of quiet flow conditions or, in other words, come from the interstream regions which are not necessarily associated with coronal holes. A final assessment of the importance of these features must await a better understanding of the structure of the lower corona and its relation to the solar wind expansion.

However, if the solar wind plasma emanates entirely from coronal hole regions and the actual electron density is less than the values tabulated by Newkirk, the ionization state freezing in positions will locate closer to the Sun. This will have two effects on the results reported above. First, due to the fact that the density gradient steepens as r decreases, the baseline used to determine a temperature gradient will shorten. This will effectively increase α as determined from the data since the freezing in temperatures deduced from ionization state abundance ratios and hence ΔT will not change. Secondly, the position of the electron temperature maximum will locate closer to the Sun and hence reduce the maximum radius of major coronal heating.

Acknowledgements

We wish to thank Drs A. Hundhausen, A. Dupree, and C. Jordan for many useful discussions. We are grateful to S. Sydoriak for programming assistance. The results reported here would not have been possible without the help of K. McCoy and P. G. Beck of the Sandia Laboratories and J. Paul Glore, H. E. Felthauser, and E. R. Tech of the Los Alamos Scientific Laboratory for engineering design and support and data handling.

The research was performed as part of the Vela satellite program, which is jointly sponsored by the U.S. Department of Defense and the U.S. Atomic Energy Commission. The program is managed by the U.S. Air Force and satellite operation activities are under the jurisdiction of the Air Force Satellite Control Facility, Sunnyvale, California.

References

Allen, J. W. and Dupree, A. K.: 1969, *Astrophys. J.* **155**, 27.
Altschuler, M. D. and Newkirk, G., Jr.: 1969, *Solar Phys.* **9**, 131.
Altschuler, M. D., Trotter, D. E., and Orral, F. Q.: 1972, *Solar Phys.* **26**, 354.
Athay, R. Grant: 1973, *Solar Phys.* **29**, 357.

Bame, S. J.: 1972, in C. P. Sonett, P. J. Coleman, Jr., and J. M. Wilcox (eds.), *Solar Wind*, NASA SP-308, p. 535.
Bame, S. J., Hundhausen, A. J., Asbridge, J. R., and Strong, I. B.: 1968, *Phys. Rev. Letters* **20**, 393.
Bame, S. J., Asbridge, J. R., Hundhausen, A. J., and Montgomery, Michael D.: 1970, *J. Geophys. Res.* **75**, 6360.
Bame, S. J., Asbridge, J. R., Feldman, W. C., and Kearney, P. D.: 1973, *Trans. Amer. Geophys. Union, EOS* **54**, 438.
Barnes, Aaron, Hartle, R. E., and Bredekamp, J. H.: 1971, *Astrophys. J.* **166**, L53.
Bevington, P. R.: 1969, *Data Reduction and Error Analysis for the Physical Sciences*, McGraw Hill Book Co., New York.
Billings, D. E.: 1966, *A Guide to the Solar Corona*, Academic Press, New York-London.
Burlaga, L. F. and Ogilvie, K. W.: 1970, *Astrophys. J.* **159**, 659.
Chapman, S.: 1957, *Smithson. Cont. Astrophys.* **2**, 1.
Davis, L., Jr.: 1965, in R. Lüst (ed.), *Stellar and Magnetic Fields* (ed. by R. Lüst) North-Holland, Amsterdam, p. 202.
Dupree, A. K.: 1972, *Astrophys. J.* **178**, 527.
Feldman, W. C., Asbridge, J. R., Bame, S. J., and Montgomery, M. D.: 1973, *J. Geophys. Res.* **78**, 2017.
Gosling, J. T., Pizzo, V. Z., and Bame, S. J.: *J. Geophys. Res.* **78**, 2001.
Hartle, R. E. and Barnes, Aaron: 1970, *J. Geophys. Res.* **75**, 6915.
Hartle, R. E. and Sturrock, P. A.: 1968, *Astrophys. J.* **151**, 1155.
Holzer, T. E. and Axford, W. I.: 1970, *J. Geophys. Res.* **75**, 6354.
House, L. L. and Billings, D. E.: 1964, *Astrophys. J.* **140**, 1182.
Hundhausen, A. J.: 1972, *Coronal Expansion and Solar Wind*, Springer-Verlag, Berlin-Heidelberg.
Hundhausen, A. J., Gilbert, H. E., and Bame, S. J.: 1968a, *Astrophys. J.* **152**, L3.
Hundhausen, A. J., Gilbert, H. E., and Bame, S. J.: 1968b, *J. Geophys. Res.* **73**, 5485.
Hundhausen, A. J., Bame, S. J., Asbridge, J. R., and Sydoriak, S. J.: 1970, *J. Geophys. Res.* **75**, 4643.
Jordan, C.: 1969, *Monthly Notices Roy. Astron. Soc.* **142**, 501.
Kearney, P. D., Asbridge, J. R., Bame, S. J., and Feldman, W. C.: 1973, *Trans. Amer. Geophys. Union, EOS* **54**, 440.
Kopp, R. A.: 1968, Thesis Harvard University, Scientific Report No. 4, AFCRL-68-0312.
Krieger, A. S., Timothy, A. F., and Roelof, E. C.: 1973, *Solar Phys.* **29**, 505.
Kuperus, M.: 1969, *Space Sci. Rev.* **9**, 713.
Lange, J. and Scherb, F.: 1970, *J. Geophys. Res.* **75**, 6350.
Mewe, R.: 1972, *Solar Phys.* **22**, 459.
Montgomery, Michael D., Asbridge, J. R., Bame, S. J., and Feldman, W. C.: 1972, *Trans. Am. Geophys. Union, EOS* **53**, 503.
Newkirk, G., Jr.: 1967, *Ann. Rev. Astron. Astrophys.* **5**, 213.
Newkirk, G., Jr.: 1972, in C. P. Sonett, P. J. Coleman, Jr., and J. M. Wilcox (eds.), *Solar Wind*, NASA SP-308, p. 11.
Noyes, R. W. and Withbroe, G. L.: 1972, *Space Sci. Rev.* **13**, 612.
Parker, E. N.: 1965, *Space Sci. Rev.* **4**, 666.
Pottasch, S. R.: 1967, *Bull. Astron. Inst. Neth.* **19**, 113.
Schatten, K. H.: 1971, *Rev. Geophys. Space Sci.* **9**, 773.
Schatten, K. H.: 1972, in C. P. Sonett, P. J. Coleman, Jr., and J. M. Wilcox (eds.), *Solar Wind*, NASA SP-308, p. 44.
Schatten, K. H., Wilcox, J. M., and Ness, N. F.: 1969, *Solar Phys.* **6**, 442.
Strong, I. B., Asbridge, J. R., Bame, S. J., Heckman, H. H., and Hundhausen, A. J.: 1966, *Phys. Rev. Letters* **16**, 631.
Sturrock, P. A. and Hartle, R. E.: 1966, *Phys. Rev. Letters* **16**, 628.
Withbroe, G. L., Dupree, A. K., Goldberg, L., Huber, M. C. E., Noyes, R. W., Parkinson, W. H., and Reeves, E. M.: 1971, *Solar Phys.* **21**, 272.